

CHARACTERIZING THE TURBULENT PROPERTIES OF THE STARLESS MOLECULAR CLOUD MBM16

PINGEL, N.M.¹, SNEZANA STANIMIROVIĆ¹, J.E.G. PEEK^{2,3}, MIN-YOUNG LEE¹, ALEX LAZARIAN¹, BLAKESLEY BURKHART¹,
AYESHA BEGUM⁴, KEVIN A. DOUGLAS⁵, CARL HEILES⁶, STEVEN J. GIBSON⁷, JANA GRCEVICH², ERIC J. KORPELA⁶,
ALLEN LAWRENCE¹, CLAIRE MURRAY¹, MARY E. PUTMAN², DESTRY SAUL²

Submitted to ApJ July 22, 2013; Accepted October 25, 2013

ABSTRACT

We investigate turbulent properties of the non-star-forming, translucent molecular cloud, MBM16 by applying the statistical technique of a two-dimensional spatial power spectrum (SPS) on the neutral hydrogen (HI) observations obtained by the Galactic Arecibo L-Band Feed Array HI (GALFA-HI) survey. The SPS, calculated over the range of spatial scales from 0.1 to 17 pc, is well represented with a single power-law function, with a slope ranging from -3.3 to -3.7 and being consistent over the velocity range of MBM16 for a fixed velocity channel thickness. However, the slope varies significantly with the velocity slice thickness, suggesting that both velocity and density contribute to HI intensity fluctuations. By using this variation we estimate the slope of 3D density fluctuations in MBM16 to be -3.7 ± 0.2 . This is significantly steeper than what has been found for HI in the Milky Way plane, the Small Magellanic Cloud, or the Magellanic Bridge, suggesting that interstellar turbulence in MBM16 is driven on scales > 17 pc and that the lack of stellar feedback could be responsible for the steep power spectrum.

Subject headings: galaxies: ISM-ISM: clouds-ISM:structure-MHD-turbulence

1. INTRODUCTION

Interstellar turbulence is expected to play a key role in the formation and evolution of structure in the interstellar medium (ISM) (McKee & Ostriker 2007). Numerous observational studies have shown that the ISM is turbulent on a vast range of scales. For instance, in the Galaxy and Magellanic Clouds, the hierarchy of spatial scales from smaller than a few parsecs to a few kiloparsecs has been observed and often attributed to interstellar turbulence (Crovisier & Dickey 1983; Green 1993; Stanimirović et al. 1999; Dickey et al. 2000). While in our current understanding many astrophysical processes require and depend on interstellar turbulence, many basic questions regarding the origin and properties of interstellar turbulence are still open. For example, what are the primary energy sources that induce turbulence over a broad range of scales? On what scales and through which modes is turbulent energy dissipated throughout the ISM? What properties of the interstellar gas determine the level and type of turbulence within the ISM (e.g. magnetic fields, galaxy mass via tidal effects, gas density and porosity)?

Statistical techniques for data analysis are very good at modeling the general properties of complex systems. In particular, the spatial power spectrum (SPS) has

been frequently used for decomposing observed images and measuring power/intensity associated with individual scales. SPS was applied to neutral hydrogen (HI) images for regions within our Galaxy (Crovisier & Dickey 1983; Green 1993; Dickey et al. 2001), for the Small Magellanic Cloud, SMC, (Stanimirović et al. 1999; Stanimirović & Lazarian 2001), the Large Magellanic Cloud, LMC, (Elmegreen et al. 2001) and the Magellanic Bridge (Muller et al. 2004). The results of these studies have shown the existence of a hierarchy of structures in the diffuse ISM, with the spectral slope varying slightly with interstellar environments. For example, HI integrated intensity images of several regions in the Milky Way, which are largely confined to the disk and likely affected by high optical depth, show a power-law slope of the SPS of ~ -3 (Lazarian & Pogosyan 2004). A slightly steeper slope of -3.4 was found for the HI column density in the SMC, and -3.7 for the LMC. The Magellanic Bridge slope (for the integrated HI intensity) varies across different regions between -2.9 and -3.5 (Muller et al. 2004). Integrated intensity maps of several gas and dust tracers have a power-law slope of -3 to -4 in the case of M33 (Combes et al. 2012). Galaxies like the LMC and M33 show a break in their power spectra, while no departure from a single power law was observed in the Galaxy, SMC and the Magellanic Bridge even at the largest probed spatial scales.

While main contributors to the interstellar turbulence and their relative importance are still not well understood, it is expected that shear from galactic rotation and large-scale gravitational/accretion flows could be responsible for large-scale energy injection in galaxies, while stellar sources (stellar outflows, winds and jets, supernovae explosions and superbubbles) inject energy on smaller scales (McCray & Snow 1979). As suggested by many numerical simulations (e.g. Vazquez-Semadeni et al. 2010), stellar feedback is expected to have a significant effect on cloud evolution resulting in an increased

¹Department of Astronomy, University of Wisconsin-Madison, 475 North Charter Street, Madison, WI 53706; pingel@astro.wisc.edu and sstanimi@astro.wisc.edu

²Department of Astronomy, Columbia University, New York, NY 10027

³Hubble Fellow

⁴Indian Institute of Science Education and Research, ITI Campus (Gas Rahat) Building, Govindpura, Bhopal- 23, India

⁵University of Calgary/Dominion Radio Astrophysical Observatory, P.O. Box 248, Penticton, BC V2A6J9, Canada

⁶Astronomy Department and Space Science Laboratory, University of California, Berkeley, CA, 94703

⁷Department of Physics and Astronomy, Western Kentucky University, Bowling Green, KY 4201

velocity dispersion and a low star formation efficiency. In addition, numerical simulations are starting to use statistical properties of the ISM (e.g. Pilkington et al. 2011) to compare simulated galaxies with observations and constrain detailed feedback processes. Clearly, observational constraints on the stellar feedback and its influence on the statistical properties of the ISM are highly desirable, yet still rare.

In this paper we investigate the importance of stellar sources for turbulent energy injection by studying the turbulent properties of the neutral hydrogen (HI) in the high-latitude ($|b| > 30^\circ$) molecular cloud MBM16 that is known to be absent of stars. We then compare our results with turbulent properties of the active stellar environments such as the SMC. Our study is largely enabled by the high resolution HI observations provided by the GALFA-HI survey (Stanimirović et al. 2006, Peek et al. 2011) which provide a wide range of spatial scales essential for applying statistical techniques.

MBM16 was first discovered by Magnani, Blitz & Mundy (1985) through CO observations at 2.6 mm. It is a large non-starforming (Magnani, LaRosa & Shore 1993), translucent (mean $A_V = 0.9$ mag, Hobbs et al. 1988) cloud at a distance of ~ 80 pc (Hobbs et al. 1988). The cloud distance was bracketed (60 to 95 pc) using interstellar Na I absorption lines in the direction of stars located behind the cloud and at varying distances. MBM16 has a mass of $320 \pm 190 M_\odot$ and is not gravitationally bound (Truong, Magnani, & Hartmann 1998). The lack of an external pressure confinement to counteract gravity suggests that the cloud’s lifetime is on the order of one Myr, which agrees with the lack of evidence for a stellar environment. The only claim of potentially stellar component associated with MBM16 is from ROSAT X-ray observations by Li, Hu & Chen (2000) who identified four potential T Tauri star candidates and concluded that future work is needed to confirm this association. In conclusion, numerous studies suggest that MBM16 has a relatively quiescent interstellar environment not polluted with current star formation.

Besides being mapped in CO (Magnani, Blitz & Mundy 1985, LaRosa, Shore & Magnani 1999) and HI (Gir, Blitz & Magnani 1994), several clumps of formaldehyde (H_2CO) were detected in absorption by Magnani, LaRosa & Shore (1993) suggesting a density of a few times 10^3 cm^{-3} at most. Regarding its large-scale environment, MBM16 is located about 10 degrees away from the Taurus molecular cloud. While several studies suggested that MBM16 could be associated with the Taurus-Auriga-Perseus complex of molecular clouds (based on the similar LSR velocity and morphology in IR images), this association is questionable considering that MBM16 is at a distance of about half that of Taurus (Hobbs et al. 1988). In general, several previous studies suggested that high-latitude translucent molecular clouds were formed in regions compressed with shocks and therefore are expected at intersections of larger gaseous (shells, sheets, flows etc) structures.

Turbulent properties of molecular gas in MBM16 were a subject of several previous studies. Magnani, LaRosa & Shore (1993) suggested that the observed properties of H_2CO clumps could be explained as a result of a large-scale shear instability. This idea was further developed

in LaRosa, Shore & Magnani (1999) who calculated the autocorrelation function of the ^{12}CO velocity field. They were able to determine a velocity correlation scale of 0.4 pc and attributed this to the formation of coherent structure due to an external shear flow. They pointed to this type of flow as a possible source for both magnetohydrodynamic (MHD) turbulence on small scales in both this and other molecular clouds. They also concluded that such flows could continuously supply kinetic energy to molecular clouds over long time scales.

More recently, Chepurnov et al. (2010) studied a high-latitude field spatially adjacent to MBM16 (RA $02^h 00^m$ to $02^h 24^m$, Dec 7° to 13° in J2000) also using GALFA-HI observations. The HI emission in the studied region was predominantly at negative velocities (-20 to 0 km s^{-1}). They applied a new statistical method, the velocity coordinate spectrum, where a one-dimensional power spectrum is derived along the velocity axis. A steep power-law slope of the velocity fluctuation spectrum of -3.9 ± 0.1 was derived, and a more shallow slope of -3.0 ± 0.1 for the power spectrum of density fluctuations. Chepurnov et al. (2010) interpreted these results as being caused by a shock-dominated turbulence.

In this paper, we apply the SPS analysis on the HI observations of MBM16 to complement previous statistical investigations, and provide a basis for future studies of high-latitude clouds from the GALFA-HI survey. The paper is structured as follows: § 2 summarizes the GALFA-HI observations and data reduction. In § 3 we summarize the basic cloud properties. In § 4, we derive the spatial power spectrum and investigate how its slope varies with velocity and velocity channel thickness, and we discuss our results in § 5.

2. DATA

The data used in this study come from the first data release of the GALFA-HI survey (DR1). GALFA-HI is a high resolution ($4'$), large area ($13,000 \text{ deg}^2$), and high spectral resolution (0.18 km s^{-1}) survey conducted with the 7-beam array of receivers ALFA at the Arecibo⁸ radio telescope. Observations were obtained using the special-purpose spectrometer GALSPECT for Galactic science. The region used for this study comes from a combination of “basket-weave” observations (PI: Peek), where the telescope is fixed at the meridian and is driven up and down in zenith angle at chosen declination (Dec) range to minimize variation of instrumental effects, and commensal “drift-scan” observations (PIs: Putman & Stanimirović, Heiles & Stanimirović), where scans at a constant declination are observed while the sky is drifting.

Data reduction of HI observations is implemented using the GALFA-HI Standard Reduction (GSR) pipeline. DR1 covers 7520 square degrees of the sky and has been produced using 3046 hours of integration time from 12 different projects. DR1 data cubes are publicly available online and a second data release is in preparation. While full details of the GSR can be found in Peek et al. (2011), we emphasize that DR1 has been calibrated for the first sidelobe contribution and further stray radiation correc-

⁸ The Arecibo Observatory is operated by SRI International under a cooperative agreement with the National Science Foundation (AST-1100968), and in alliance with Ana G. Mendez-Universidad Metropolitana, and the Universities Space Research Association.

tion (due to more distant sidelobes) is planned for future data releases. The estimated contribution of the stray radiation is < 1 K for the region of interest in this study (based on the comparison with well calibrated surveys). This has negligible effect on the results of our SPS analysis in Section 4 as the HI emission under investigation is very bright (e.g. Figure 5).

Our region of interest extends from RA $2^h 50^m$ to $3^h 45^m$, Dec 4° to 16° (J2000). The rms noise measured in the extracted data cube over emission-free channels is $\sigma = 0.43$ K at the original velocity resolution of 0.18 km s $^{-1}$. Please note that in the SPS analysis (Section 4) where we average several velocity channels we re-calculate the rms noise before estimating the uncertainty for the HI column density.

3. OBSERVATIONAL RESULTS

The region under investigation in this study encompasses the CO emission from LaRosa, Shore, & Magnani (1999) but is significantly more extended. This is shown in Figure 1 where in grey-scale we show the HI emission at the velocity of the peak CO intensity, with CO integrated intensity overplotted in white. The HI emission essentially forms an arc-like feature, with the CO map covering the arc's deflection point. However, there are indications that CO may be more extended than what is shown by LaRosa, Shore, & Magnani (1999). We have added here as crosses six CO detections from Magnani et al. (2000) from an unbiased CO survey of the southern Galactic hemisphere with the 1.2m CfA telescope. While four crosses are coincident with white contours, two detections are located just outside the traditionally considered CO boundary of MBM16. All of the HI emission shown in Figure 1 is included in our analysis.

The average HI profile for the whole area shown in Figure 1 is shown in Figure 2 (black), together with the average, scaled ^{12}CO ($J = 1-0$) profile from LaRosa, Shore, & Magnani (1999) (red). This shows that HI is more extended than CO, similar to what has been seen for many other molecular clouds. This averaged HI profile appears to have two Gaussian components based on least-squares fitting. The stronger Gaussian component, with the peak brightness temperature of 39 ± 2 K, agrees well with the molecular component in terms of its velocity center (8 km s $^{-1}$) and range (4 to 10 km s $^{-1}$, FWHM of 9.9 ± 0.3 km s $^{-1}$). The smaller Gaussian component peaks at a brightness temperature of 20 ± 1 K and has a FWHM of 16.4 ± 0.8 km s $^{-1}$. LaRosa, Shore, & Magnani (1999) also noticed a weaker molecular cloud between -20 and -5 km s $^{-1}$. While the distance of this second cloud is not known, it could be associated with the second (weaker) Gaussian HI component.

In Figure 3 we show an image obtained after integrating the HI data cube along the RA axis calculated over the whole region of interest. While a small amount of gas is present at negative LSR velocities, across most of the spatial extent the main velocity component dominates and is well-centered at ~ 8 km s $^{-1}$. The negative-velocity component is not obvious in this image as it has a localized spatial extent. It is centered at about five degrees south of the center of the CO emission in a cloud-like feature about 2 degrees in diameter. To ensure that all velocity channels used for SPS analysis in

the next section are filled with HI emission we restrict the velocity range for our study to -2 to 16 km s $^{-1}$. This range corresponds to the full width at half maximum of the integrated velocity profile in Figure 2. We note that repeating our SPS analysis on the full velocity range of -20 to 20 km s $^{-1}$ does not result in significant differences.

A column density image integrated over -2 to 16 km s $^{-1}$ under the assumption of optically thin HI is shown in Figure 4 with the minimum and maximum column density measurements being 4.7×10^{20} and 2.2×10^{21} cm $^{-2}$, respectively. Our derived mean HI column density of $9.3 \pm 3.4 \times 10^{20}$ cm $^{-2}$ agrees well with an average value of 9.3×10^{20} cm $^{-2}$ measured by Gir, Blitz & Magnani (1994) using the Green Bank 43 m telescope. Figure 5 shows a peak intensity image of HI associated with MBM16, and reveals the range of HI morphology of MBM16. Some regions, most notably the center, are smooth and continuous, while filamentary structure is present towards the edge of the image with sharp transitions between high and low brightness temperature values.

4. SPATIAL POWER SPECTRUM

4.1. Derivation of the SPS

Our methodology for deriving the SPS is similar to previous studies (Crovisier & Dickey 1983; Green 1993; Stanimirović et al. 1999; Stanimirović & Lazarian 2001; Elmegreen et al. 2001; Muller et al. 2004). We begin with two-dimensional images of the HI intensity measurements (I). Stanimirović & Lazarian (2001) define the 2D spatial power spectrum as:

$$P(k) = \int \int \langle I(x) I(x') \rangle e^{i\mathbf{L}\cdot\mathbf{k}} d\mathbf{L}, \quad \mathbf{L} = \mathbf{x} - \mathbf{x}' \quad (1)$$

with \mathbf{k} being the spatial frequency, measured in units of wavelength and is $\propto 1/l$ where l is the length scale, and \mathbf{L} being the distance between two points. This is essentially the Fourier Transform of the auto-correlation function of the HI intensity fluctuations. We take the Fourier Transform of the intensity images and square the modulus of the transform — $\langle \Re^2 + \Im^2 \rangle$, where \Re and \Im are the real and imaginary components, respectively — to obtain the power spectrum image, which we refer to as the modulus image. Thirteen annuli of equal width originating at the center of the modulus image are then overlaid at logarithmic intervals, as shown in Figure 6. Each successive annulus corresponds to a certain linear scale in the intensity image. Larger annuli probe the amount of power at smaller spatial scales, while the smaller annuli probe the largest spatial scales within MBM16. To measure the average power per annulus we assume azimuthal symmetry and calculate the median value for each annulus. The use of median is motivated by the fact that the modulus image has very bright pixels along the central axes caused by the Gibbs phenomenon, in which the Fourier series sum oscillates around discontinuities, and leads to $\sin(x)/x$ ringing resulting from the sharp image edges (Figure 6). While we have experimented with tapering of the original images so the intensity decreases smoothly to zero at the edges, the distribution of data values in each annulus is well behaved with the majority of data points following a Gaussian distribution and ringing only introducing a high-end tail of the distribu-

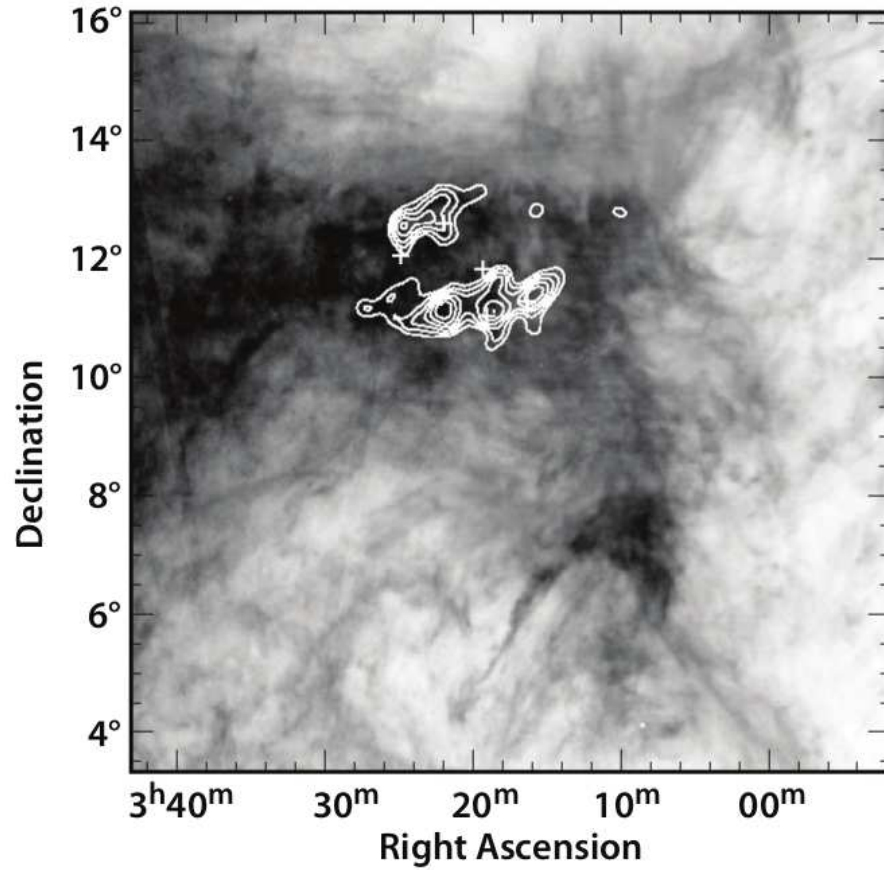


FIG. 1.— An HI emission image of MBM16 at a velocity of 8 km s^{-1} (LSR). The CO integrated intensity from LaRosa, Shore, & Magnani (1999) is shown with white contours from 40% to 90% with steps of 10% of total intensity. Crosses are CO detections from Magnani et al. (2000).

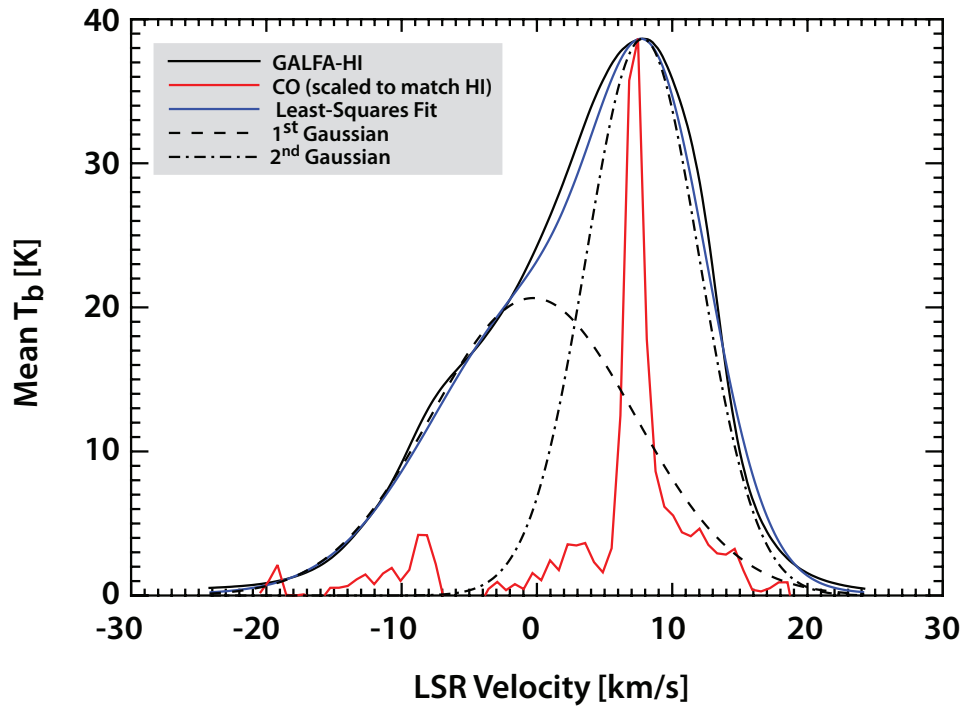


FIG. 2.— The mean HI profile of MBM16 (black) and the scaled CO spectrum (red) highlighting the velocity range of the data set used. Two fitted Gaussian functions are shown as dashed lines and the combined fit is shown in blue.

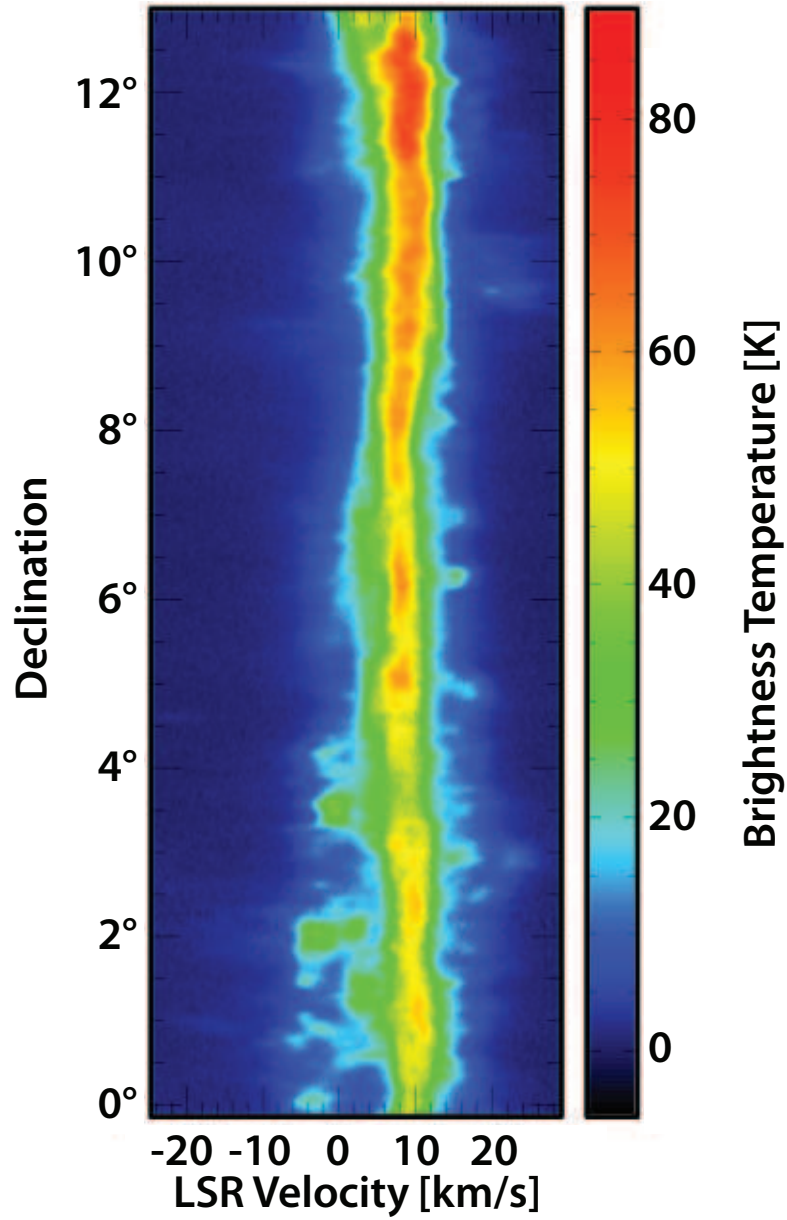


FIG. 3.— The integrated intensity image along the RA axis of the region shown in Figure 1. HI between -5 and -10 km s^{-1} may be associated with a separate molecular cloud (LaRosa, Shore, & Magnani 1999) located at a different distance than MBM16.

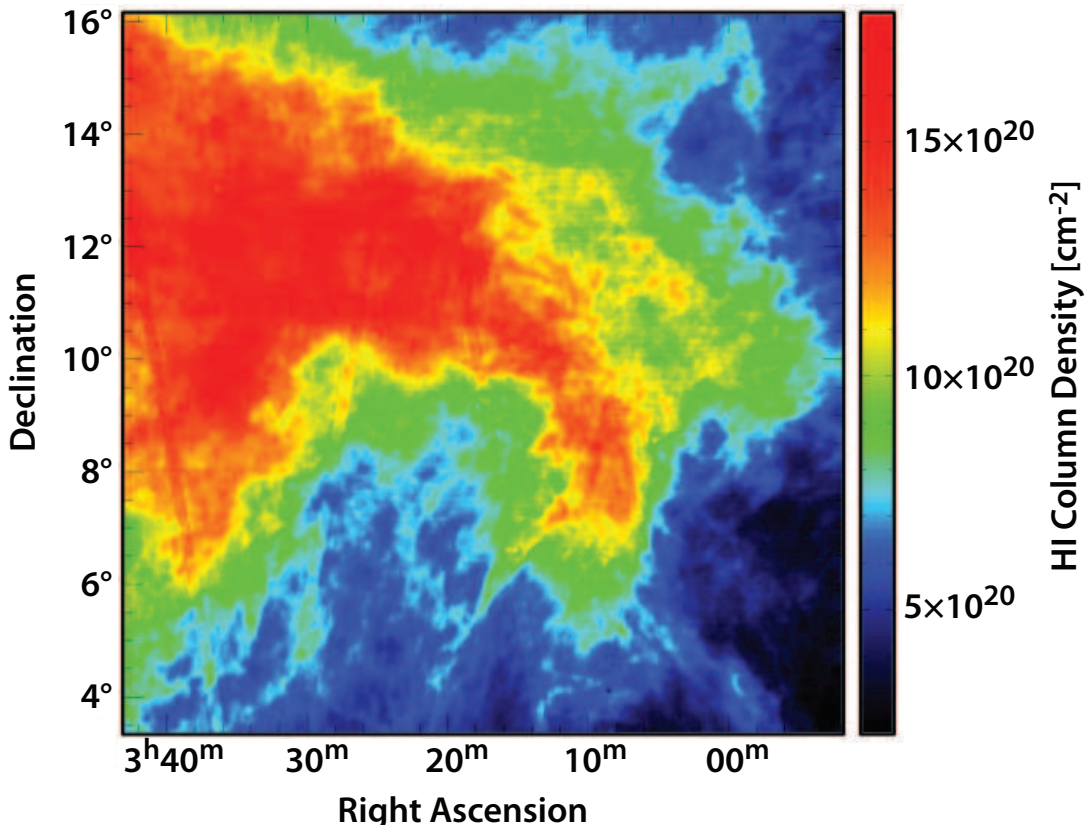


FIG. 4.— The HI column density image of MBM16 in units of (cm^{-2}) integrated over -2 to 16 km s^{-1} . The physical scales range from 0.1 pc for the beam size to $\sim 17 \text{ pc}$ for the size of the entire region.

tion. Therefore, the average power per annulus is well-represented with the median value. This median power is then plotted as a function of spatial scale, as shown in Figures 7-8.

To estimate the error in calculating the median power for each spatial scale we perform a Monte Carlo simulation. Based on our estimated uncertainty for image intensity (brightness temperature) per individual velocity channel, we generate 1000 HI intensity images by using 1000 intensity values for each image pixel, randomly drawn from a Gaussian distribution centered on the original pixel's value, and a standard deviation being equal σ (where σ is the measured rms noise per individual velocity channel). From here, for each annulus, we measure 1000 median values, and estimate the final uncertainty as the standard deviation of these 1000 median values. These uncertainties range in value from four to two orders of magnitude below the calculated median power for a given spatial scale. The uncertainties are shown in Figure 7 but are generally too small to be noticed. When integrating over several velocity channels in Section 4.2 the standard deviation used in the Monte Carlo simulation is calculated as: $\sigma \times \sqrt{N} \times \Delta v$, where N is the number of channels being averaged and Δv is the original velocity width of a single channel.

In addition to the above random uncertainties we also investigate the power spectrum of our emission-free channels in the data cube. In the case that there are no systematic errors associated with temperature calibration and/or imaging, the noise power spectrum should be flat. According to Green (1993), the observed power spectrum

at a particular spatial frequency k can be written as:

$$P_{obs}(k) = P_{HI}(k) + P_{noise}(k) \quad (2)$$

where P_{HI} is the pure HI power spectrum and P_{noise} is the noise-only contribution (assuming no absorption). An example emission-free power spectrum is shown in Figure 7 using square symbols. While this spectrum shows the existence of some residual power at larger-scales, likely caused by imperfections in the gain calibration, the noise power observed is 3-4 orders of magnitude smaller than the power measured in emission channels. Therefore, subtracting the noise power spectrum from the derived emission spectrum and re-fitting leads to a negligible change in the power-law slope of 0.1% . We therefore conclude that this residual noise mainly on scales 5-17 pc is not affecting our results.

4.2. SPS Results

We begin by showing a few example power spectra calculated over the whole velocity range of interest -2 to 16 km s^{-1} for velocity channels averaged over 2.9 km s^{-1} (Figure 8), in order to obtain six equally wide velocity slices. With the distance to MBM16 estimated to be approximately 80 pc (Hobbs et al. 1988) and an angular resolution of the GALFA-HI survey equal to $4'$, the spatial frequency can directly relate to physical size. This is plotted on the x-axis and our observations cover a range of spatial scales from 0.1 pc to 17 pc . The power spectra can clearly be fitted with a power-law function, $P(k) \propto k^\gamma$, and are very well behaved over the whole velocity range. We fit a non-weighted power-law function.

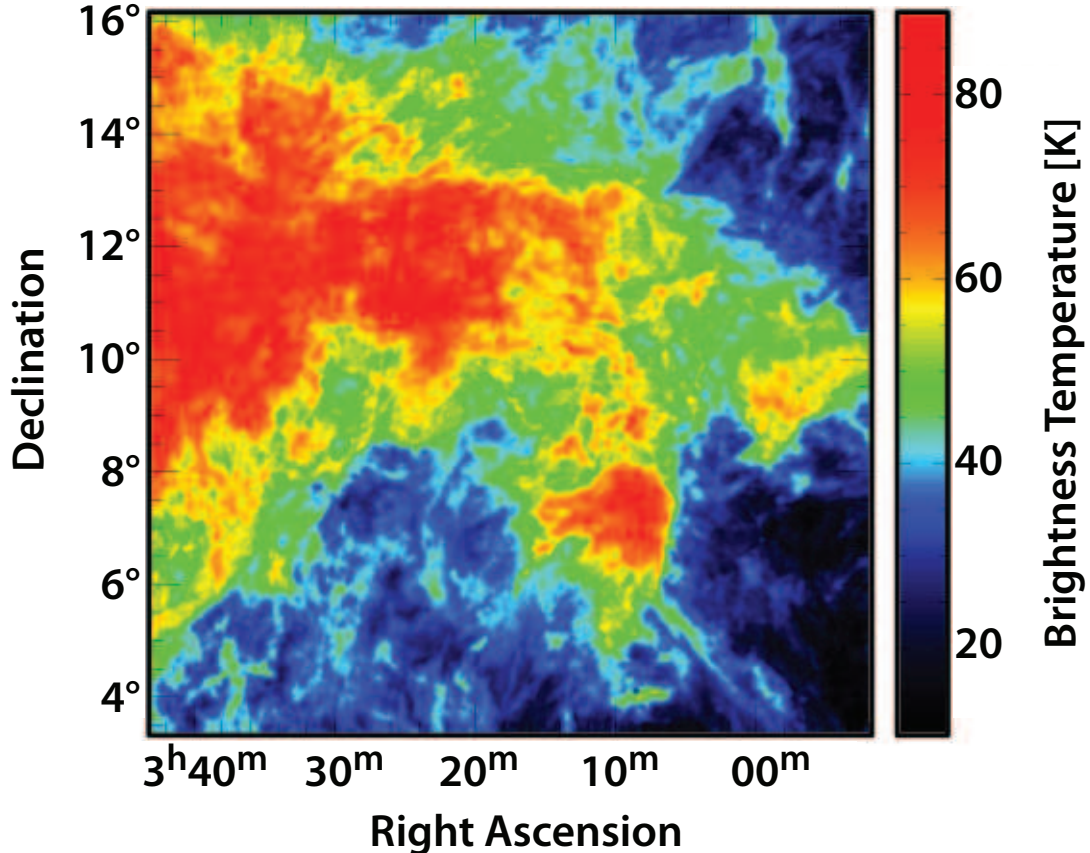


FIG. 5.— The peak HI brightness temperature image calculated over the velocity range of -2 to 16 km s^{-1} .

To estimate the uncertainty for each fit, we iteratively remove one data point and refit. The uncertainty on the power-law slope is then calculated as the weighted standard deviation of the derived slopes. The weighted average slope for these six panels is $\langle \gamma \rangle = -3.58 \pm 0.09$.

To investigate whether the power-law slope varies with individual velocity channels, for a given (fixed) velocity channel width, we show in Figure 9 the power-law slope as a function of the LSR velocity measured for velocity thickness $\Delta v = 0.72 \text{ km s}^{-1}$, which correspond to twenty-four individual velocity slices. Within the estimated fitting uncertainties, the power-slope is essentially constant for a fixed velocity thickness.

As suggested in Lazarian & Pogosyan (2000), hereby referred as LP00, intensity fluctuations seen in the HI images result from a combination of both velocity and density fluctuations, commonly referred to as $P_v \propto k^{-3-m}$ and $P_s \propto k^n$. By integrating a spectral-line data cube over a varying range of velocity intervals (or channels), the relative contributions of velocity and density fluctuations are expected to vary in a systematic way, allowing derivation of power-law indices corresponding to density and velocity fields separately (n and m). Due to this dependence of intensity fluctuations on both velocity and density fluctuations, the power-law index is expected to be a function of velocity slice thickness, i.e. $\gamma(\Delta v)$. At small Δv the velocity fluctuations have a considerable effect on the measured power-law index, resulting from velocity flows pushing emission into adjacent velocity channels (Muller et al. 2004). However, LP00

showed that these velocity fluctuations can be averaged out by integrating over wider velocity ranges. At the largest Δv the velocity fluctuations tend to be averaged out, leaving only the contributions from the underlying three-dimensional density structure contributing to the measured power-law index.

Based on the above expectations, we investigate how the power-law slope depends on the thickness of our velocity channels Δv . We start with the full data cube (with individual channels having $\Delta v = 0.18 \text{ km s}^{-1}$), calculate the power spectrum and its power-law slope for each individual velocity channel, calculate the weighted-mean slope for each channel, and then gradually average several velocity channels together to increase Δv all the way to the whole cube being compressed to a single velocity channel of $\Delta v \sim 18 \text{ km s}^{-1}$. We then plot the weighted average with 1σ uncertainties as a function of Δv in Figure 10.

It is clear that the average power-spectrum slope becomes gradually steeper as velocity slice thickness increases, and flattens around $\Delta v \sim 5 - 10 \text{ km s}^{-1}$. Based on LP00, this suggests that both velocity and density fluctuations contribute to the intensity fluctuations in the intensity images, especially at narrow velocity channels. This observed trend is in agreement with the LP00 predictions, and suggests the 3D slope of density fluctuations $n = -3.7 \pm 0.2$. The measured SPS slope at the smallest velocity width contains information about velocity fluctuations. LP00 predict that $\gamma(\Delta v)$ should also converge or flatten at this end of velocity slice thickness.

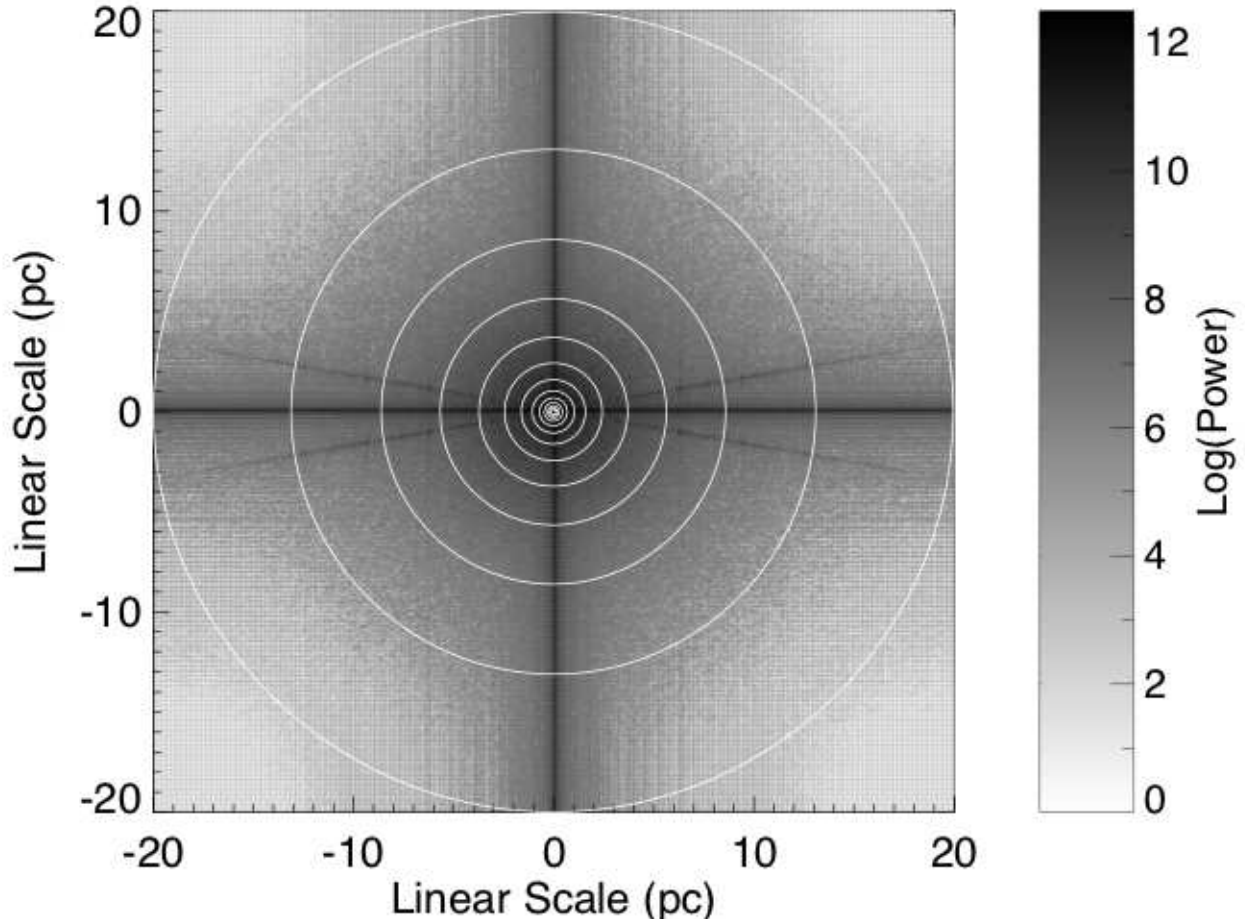


FIG. 6.— An example modulus image, $\langle \Re^2 + \Im^2 \rangle$, used to measure the spatial power spectrum. Very bright pixels along the central axes are caused by sharp image edges, so called Gibbs phenomenon. The bright lines inclined at an angle of about 15 degrees relative to the x-axis correspond to the low-level imperfections in the gain calibration of our basket-weave scanning tracks (Section 4.1).

However, we do not observe this flattening in Figure 10. This suggests that even our smallest $\Delta v \sim 0.18 \text{ km s}^{-1}$ is still not probing the predominantly “thin” velocity slices largely dominated by velocity fluctuations. Therefore, based on LP00, if the most shallow slope we measure corresponds to an intermediate velocity slice thickness case then $\gamma = -3 - m/2 \sim -3.3$ and we get $m \sim 0.6$ and the 3D velocity spectrum $P_v \propto k^{-3.6}$. However, if this slope corresponds to a “thin” slice case, then $\gamma = -3 + m/2 \sim -3.3$ and we get $m \sim -0.6$ and $P_v \propto k^{-2.4}$.

5. DISCUSSION

The spatial power spectrum of HI associated with MBM16 shows a power-law behavior with a relatively constant power-law slope across the cloud velocity range and for a fixed velocity channel thickness. This is similar to power spectra derived for the Galaxy (Crovisier & Dickey 1983; Green 1993), for the SMC (Stanimirović et al. 1999; Stanimirović & Lazarian 2001), and the Magellanic Bridge (Muller et al. 2004) in that they are well fit by a single power-law function.

The slope of the power spectrum varies with the thickness of velocity channels, in agreement with the LP00 predictions. The estimated 3D slope of density fluctuations is steep at $n = -3.7 \pm 0.2$, essentially identical to the Kolmogorov $-11/3$ slope expected for incompressible

turbulence with energy injection on large scales only and dissipation at small scales. Our rough estimate of the 3D velocity spectrum suggests $P_v \propto k^{-2.4}$ to -3.6 (for the case of Kolmogorov turbulence $P_v \propto k^{-3.7}$). However, as we do not detect the saturation of the power-spectrum slope at small Δv our velocity slope is not well determined. As the power spectra do not show evidence for a turnover on large spatial scales, this suggests that turbulence is being driven on scales larger than 17 pc.

The most interesting result from this analysis is that the estimated 3D slope of density fluctuations in MBM16 ($n = 3.7 \pm 0.2$) is significantly steeper than the slope obtained for several regions in the Milky Way plane (Crovisier & Dickey 1983; Green 1993; Khalil et al. 2006), the SMC, the Magellanic Bridge, and several other galaxies (e.g. for the SMC $n = -3.30 \pm 0.01$, while the slope of the velocity spectrum is ~ -3.4). The difference could result from the lack of turbulent energy injection at small scales from stellar feedback in MBM16, therefore providing evidence that stellar feedback provides important contribution to turbulent energy in the ISM.

Previous studies of MBM16’s velocity autocorrelation (Magnani, LaRosa, & Shore 1993; LaRosa, Shore, & Magnani 1999) from CO observations revealed evidence for transient coherent structure in the molecular gas and suggested that an external shear flow, arising at the

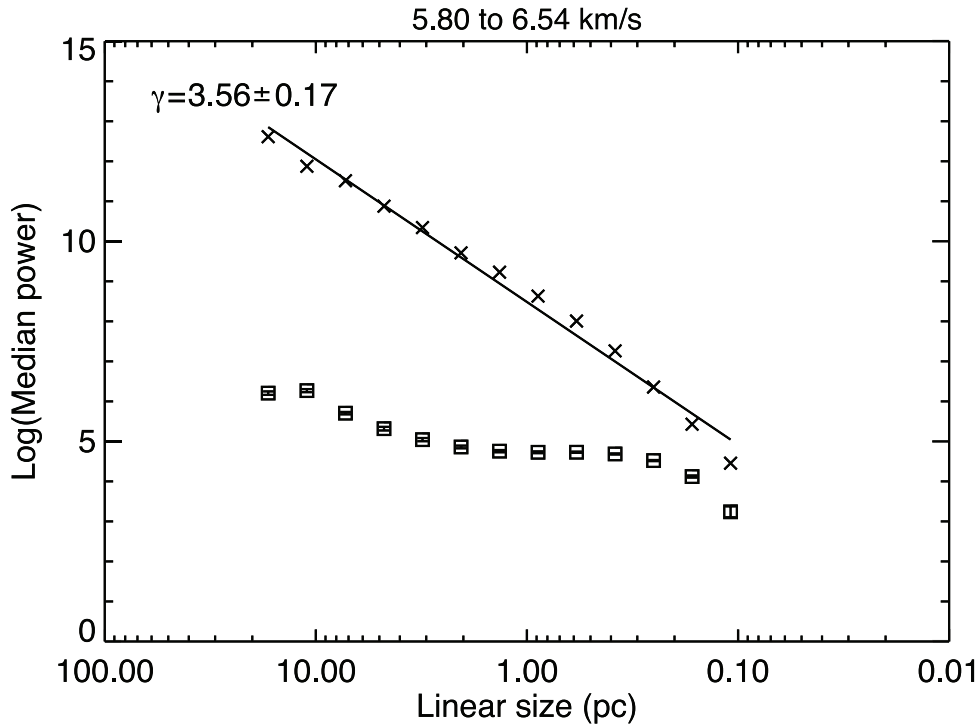


FIG. 7.— An example power spectrum calculated for HI images over the velocity range of 5.8 to -6.5 km s $^{-1}$. The power-law fit is overlaid. Due to the small errors associated with calculating the median power, the error in the fit is determined by removing one data point at the time, re-fitting the power spectrum, and estimating the maximum deviation of the derived slopes. The SPS shown with squares was derived using only emission-free channels in the data cube over a velocity width of 0.72 km s $^{-1}$.

boundary layer between MBM16 and the surrounding ISM, powers the turbulent velocity field in this high-latitude cloud. The lack of observed turnover in the HI power spectrum agrees with the scenario that turbulent energy is being introduced on the spatial scales larger than 17 pc in MBM16. Being non self-gravitating and located about ~ 50 pc above the Milky Way plane, MBM16’s interstellar environment resembles conditions found in outer galaxy disks where shear due to Galactic rotation can initiate the magnetorotational instability, which in turn drives turbulence on large scales (Piontek & Ostriker 2007). Alternatively, as suggested and modeled by Keto & Lattanzio (1989), collisions between high-latitude clouds can induce gravitational instability and turbulence needed to also explain broad CO linewidths commonly observed in these clouds.

The estimated spectral indices agree very well with results from another high-latitude field, in Ursa Major, by Miville-Deschenes et al. (2003) who derived -3.6 ± 0.2 for the slope of the HI column density fluctuations over the range of scales from 0.5 to 25 pc. In addition, they measured the same slope for the power spectrum of the HI velocity centroid field. While our velocity fluctuation spectrum is in rough agreement with results from Chepurnov et al. (2010) for an adjacent high-latitude field, our density slope is significantly steeper.

We can also compare our derived SPS slope with the prediction from isothermal MHD simulations. Figure 10 of Burkhart et al. (2010) plots the SPS slope for density fluctuations derived from isothermal simulations as a function of sonic Mach number \mathcal{M}_s for super-Alfvénic ($\mathcal{M}_A = 0.7$) and sub-Alfvénic ($\mathcal{M}_A = 2.0$) simulations. The SPS slope becomes more shallow with in-

creasing \mathcal{M}_s . For any given \mathcal{M}_A the slope is steeper for sub-Alfvénic turbulence. However, regardless of the super-Alfvénic or sub-Alfvénic case, a very steep slope of ~ -3.7 is expected only in the case of sub-sonic or transonic medium with $\mathcal{M}_s < 2$. While MBM16 certainly has a mixture of warm and cold HI phases, if the warm medium dominates in terms of its fraction, then the observed HI power spectrum suggests a sub-sonic or transonic HI in MBM16.

In summary, we have used the two-dimensional SPS on high-resolution HI observations to investigate the internal turbulence of the non-starforming, translucent molecular cloud, MBM16. By fixing the velocity slice thickness we find that the HI power spectrum is well represented with a power-law function, with the slope γ staying relatively constant throughout the full velocity range for the cloud. By treating γ as a function of velocity slice thickness, we find that the average value of the slopes is influenced by velocity fluctuations at small Δv , while at large Δv the influence from velocity has been averaged out to leave density fluctuations as the dominant mechanism for the observed intensity fluctuations. The slope of HI density fluctuations is estimated as $n = -3.7 \pm 0.2$, which is steeper than the density spectral index obtained for the Galaxy, the SMC, and the Magellanic Bridge. This result for a starless environment suggests that stellar feedback may play a prominent role in turbulent energy injection on spatial scales 0.1 - 10 pc. It will be very interesting to see if future studies of starless clouds support our finding.

The authors would like to thank Steve Shore for providing the CO observations of MBM16, and an anyo-

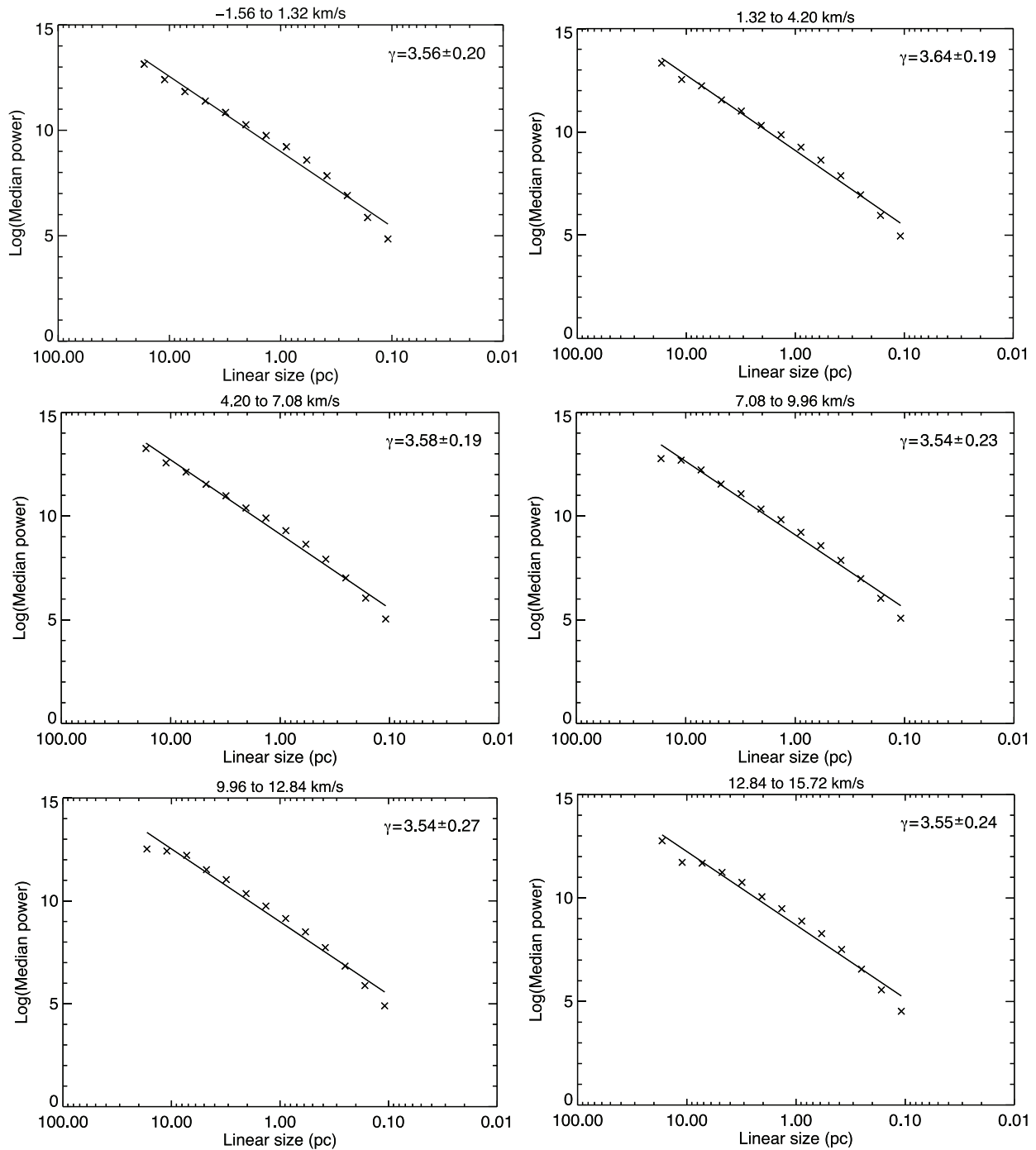


FIG. 8.— Example power spectra of velocity slices, each slice is the average of 16 velocity channels from the original HI data cube, with $\Delta v = 2.9 \text{ km s}^{-1}$. The weighted mean of the six power-law slopes shown here is -3.58 ± 0.09 .

mous referee for providing constructive suggestions. N.P., S. S., M.-Y.L., M.E.P., C.H., E.J.K., J.E.G.P., A.B., J.G., and D.S. acknowledge support from NSF grants AST-0707597, 0917810, 0707679, and 0709347. N.P., M.-Y.L. and S.S. thank the Research Corporation for Science Advancement for their support. J.E.G.P. was supported by HST-HF-51295.01A, provided by NASA

through a Hubble Fellowship grant from STScI, which is operated by AURA under NASA contract NAS5-26555. We credit the use of the KARMA visualization software package (Gooch 1996)⁹. visualization software (Gooch 1996).

REFERENCES

Burkhart, B., Stanimirović, S., Lazarian, A., and Kowal, G., 2010, *ApJ*, 708, 1204

⁹ See also <http://www.atnf.csiro.au/karma>.

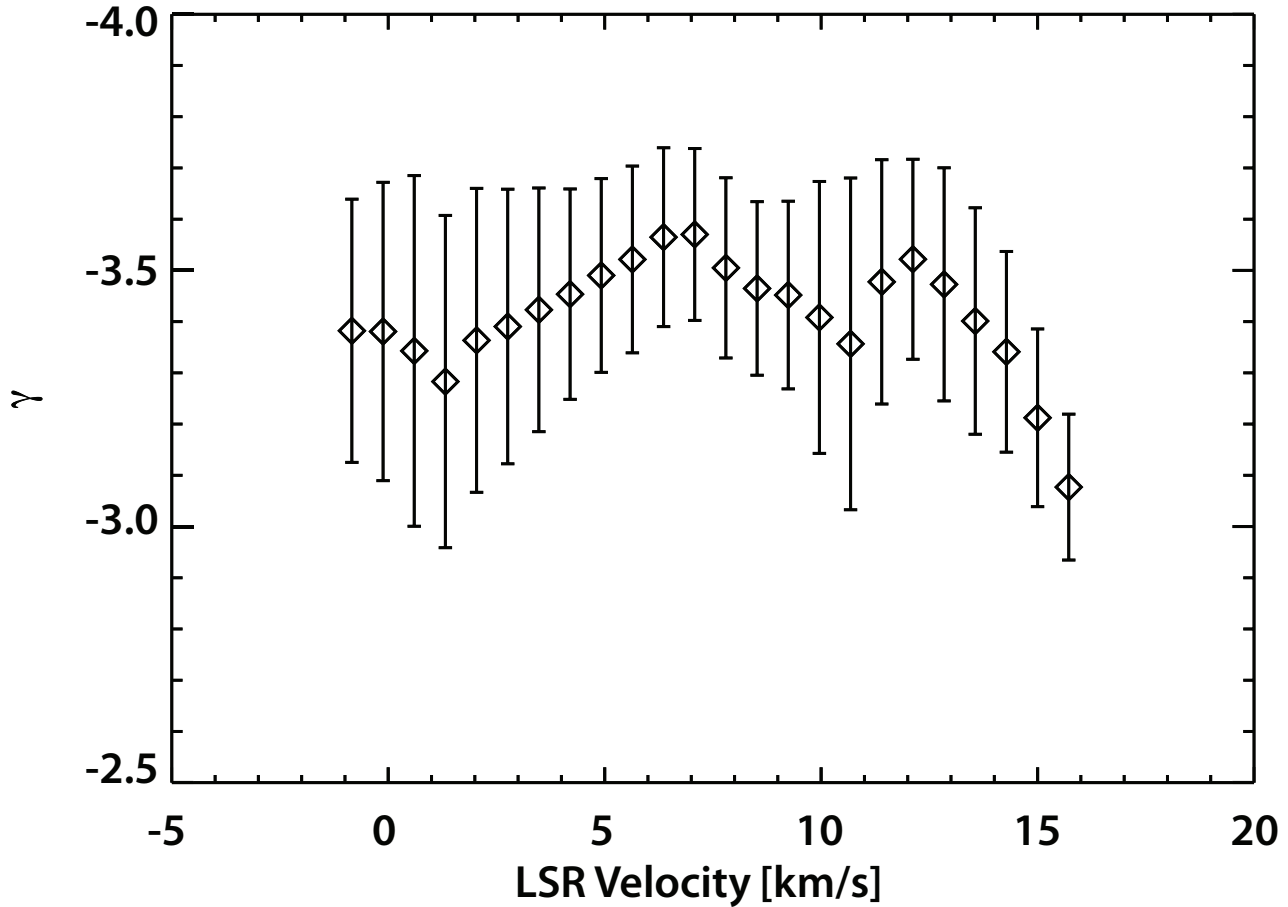


FIG. 9.— The power spectrum slope vs. the LSR velocity of MBM16 for 24 velocity slices each with $\Delta v = 0.72 \text{ km s}^{-1}$. Note the relatively constant slope over the velocities corresponding to the bulk of emission.

- Chepurnov, A., Lazarian, A., Stanimirović, S., Heiles, C. and Peek, J. E. G., 2010, *ApJ*, 714, 1398
- Combes F. et al., 2012, *A&A*, 539, A67
- Crovisier, J. and Dickey, J. M. 1983, *A&A*, 122, 282
- Dickey, J. M., McClure-Griffiths, N. M, Stanimirović, S., Gaensler, B. M., and Green, A. J., 2001, *ApJ*, 561, 264
- Dickey, J., Mebold, U. Stanimirović, S., & Staveley-Smith, L. 2000, *ApJ*, 536, 756
- Elmegreen, B. G., Kim, S., & Staveley-Smith, L., 2001, *ApJ*, 549, 749
- Gir, B. Y., Blitz, L., Magnani, L. 1994, *ApJ*, 434, 162
- Gooch, R. 1996, ASP Conf. Ser. 101, *Astronomical Data Analysis Software and Systems V*, eds. G. H. Jacoby & J. Barnes, 80
- Green D.A., 1993, *MNRAS*, 262, 327
- Hobbs, L. M., Penprase, B.E., Welty, D.E., Blitz, L., and Magnani, L. 1988, *ApJ*, 327, 356
- Keto, E. R. & Lattanzio, J. C. 1989, *ApJ*346, 184
- Khalil, A., Joncas, G., Nekka, F., Kestener, P. & Arneodo, A. 2006, *ApJ*, 165, 512
- Larosa, T. N., Shore, S.N., and Magnani, L. 1999, *ApJ*, 512, 761
- Lazarian, A., & Pogosyan, D. 2000, *ApJ*, 537, 720
- Lazarian, A., & Pogosyan, D. 2004, *ApJ*, 616, 943
- Li, J. Z., Hu, J. Y., & Chen, W. .P, 2000, *A&A*, 356, 157
- Magnani, L., Blitz, L., and Mundy, L., 1985, *ApJ*, 295, 402
- Magnani, L., LaRosa, T. N., & Shore, S. N., 1993, *ApJ*, 402, 226
- Magnani, L., Hartmann, D., Holcomb, S.L., Smith, L.E., & Thaddeus, P., 2000, *ApJ*, 535, 167
- McCray, R. & Snow, Jr., T. P., 1979, *ARA&A*, 17, 213
- McKee, C.F., & Ostriker, E. C. 2007, *ARA&A*, 45, 565
- Miville-Deschênes, M. A., Joncas, G., Falgarone, E. and Boulanger, F., 2003, *A&A*, 411, 109
- Muller, E., Stanimirović, S., Rosolowsky, E., & Staveley-Smith, L. 2004, *ApJ*, 616, 845
- Peek, J.E.G., Heiles, C., Douglas, K.A., Lee, M.-Y., Grcevich, J., Stanimirović, S., Putman, M.E., Korpela, E.J., Gibson, S.J., Begum, A., Saul, D., Robishaw, T., and Krčić, M. 2010, *ApJS*, 194, 20
- Pilkington K., Gibson B. K., Brook C. B., Calura F., Stinson G. S., Thacker R. J., Michel-Dansac L., Bailin J., Couchman H. M. P., Wadsley J., Quinn T. R., Maccio A., 2011, *MNRAS*, 425, 969
- Piontek, R.A. & Ostriker, E.C. 2007, *ApJ*, 663, 183
- Stanimirović, S. & Lazarian, A. 2001, *ApJ*, 551, L53
- Stanimirović, S., Putman, M., Heiles, C., et al. 2006, *ApJ*, 653, 1210
- Stanimirović, S., Staveley-Smith, L., Sault, R. J., Dickey, J. M., & Snowden, S. L. 1999a, *MNRAS*, 302, 417
- Truong, A. T.; Magnani, L.; Hartmann, D. 1997, in *Bull. Am. Astron. Soc* 29, *The Gravitational Stability of MBM16*, (Washington DC: AAS), 1220
- Vazquez-Semadeni, E., 2010, *Astronomical Society of the Pacific Conference Series* 438, *Molecular Cloud Evolution*, ed Kothes, R., Landecker, T. L., Willis, A.G., (Naramata, British Columbia, Canada: ASPC), 83

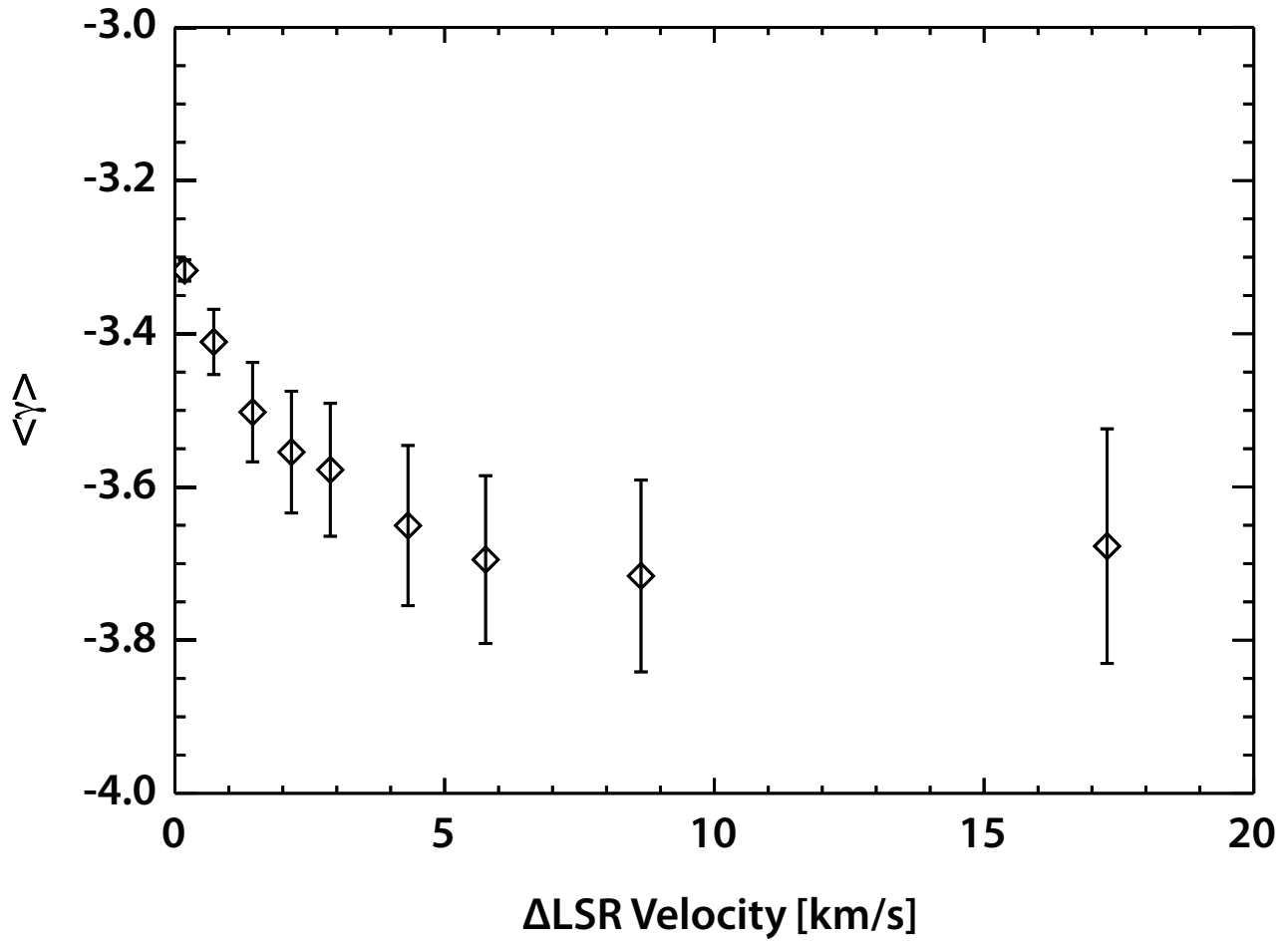


FIG. 10.— Variation of the two-dimensional HI power spectrum slope, $\langle \gamma \rangle$, with velocity slice thickness Δv .